The Capillary Flow Experiments aboard ISS: Moving Contact Line Experiments and Numerical Analysis

Mark M. Weislogel[1] and Ryan M. Jenson[2]
Portland State University, Portland, OR 97207

Jörg Klatte[3] and Michael E. Dreyer[4]
Center for Applied Space Technology and Microgravity, University of Bremen, Bremen 28359

This paper serves as a first presentation of quantitative data reduced from the Capillary Flow Contact Line Experiments recently completed aboard the International Space Station during Expeditions 9-16, 8/2004-11/2007. The simple fluid interface experiments probe the uncertain impact of the boundary condition at the contact line—the region where liquid, gas, and solid meet. This region controls perhaps the most significant static and dynamic characteristics of the large length scale capillary phenomena critical to most multiphase fluids management systems aboard spacecraft. Differences in fluid behavior of nearly identical static interfaces to nearly identical perturbations are attributed primarily to differences in fluid physics in the vicinity of the contact line. Free and pinned contact lines, large and small contact angles, and linear and nonlinear perturbations are tested for a variety of perturbation types (i.e. axial, slosh, and other modes) to right circular cylinders. The video and digitized datasets are to be made publicly available for model benchmarking. In parallel with the experimental effort, blind numerical predictions of the dynamic interface response to the experimentally applied input perturbations are offered as a demonstration of current capabilities to predict such phenomena. The agreement and lack of agreement between the experiments and numerics is our best guide to improve and/or verify current analytical methods to predict such phenomena critical to spacecraft fluid systems design.

I. Introduction: The Capillary Flow Experiment—Contact Line (CFE-CL)

CAPILLARY flows and phenomena are critical to many important fluids management systems in low-g environments such as fuels/cryogen storage systems, thermal control systems (e.g., vapor/liquid separation), life support systems (e.g., water recycling), and other materials processing in the liquid state. Under microgravity conditions, the impact of dominant capillary forces must be well understood if such large mission-critical systems are to perform predictably. To enhance such understanding, the Capillary Flow Experiments (CFE) aboard the International Space Station (ISS) are designed as a collection of quantitative fundamental and applied capillary phenomena experiments conducted using handheld hardware. The experiments address certain aspects of interface dynamics and stability (CFE-CL, two vessels each), critical geometric wetting (CFE-VG, 2 each), and 3-D wicking (CFE-ICF, 2 each). The general aim of CFE is to provide results of incremental value to the low-g fluid systems design community that cannot be readily obtained in ground-based tests. Specific applications of the results largely center on particular fluids challenges concerning liquids management. Results from the CFE-CL (CL) experiments are reported here. Further CFE details may be found in Refs. 1-3 and a complete NASA technical memorandum is forthcoming.

II. Motivation and Overview

Knowledge of the curvature of a capillary dominated fluid interface is central to understanding both the static and dynamic behavior of the interface and in turn the locations of the fluid phases it divides. For example, the liquid center of mass (i.e. location), natural frequency, damping, and stability all depend critically on the base state static or

[1]Professor, Department of Mechanical Engineering, P.O. Box 751-ME, member.
[2]M.S.M.E. Candidate, Department of Mechanical Engineering, P.O. Box 751-ME.
[3]Ph.D. Candidate, Research Scientist, Am Fallturm, Bremen Germany.
[4]Sr. Scientist, Professor, Am Fallturm, Bremen Germany.

dynamic curvature of the interface. Unfortunately, such curvature in turn depends critically on the particular wetting conditions at the contact line—the absence of an accurate physical description of which remains a potentially serious design impediment. Over the past 40 years numerous authors have reviewed the fertile research field of static and dynamic wetting and the pivotal role of the moving contact line boundary condition[4-8]. Despite the literature being replete with insightful studies the seemingly limitless variety of wetting surfaces and scenarios tend to overwhelm the designer who is perhaps more interested in a boundary condition that merely produces design specific results than in a boundary condition that is actually physically correct. The establishment of the latter may still be decades away despite significant recent achievements[9]. In the meantime, the low-g fluids systems designer is faced with computing large-scale interfacial phenomena (large length ~ O(m), large mass ~ O(tons)) potentially critically dependent on an ill-defined micro-scale boundary condition at the moving contact line. Some argue that this shortcoming is of little consequence and that present methods are adequate[10]. The present study seeks to report when such a perspective is appropriate and of course, and of equal importance, when it is not.

Standing alone, the CL experiments provide in part a low-g dataset useful in comparing extremes in dynamic contact line conditions. However, the results are perhaps most suitable for model benchmarking. The dynamic interface experiments employ partially filled right circular cylinders for which a large ground-based low-g experiment history is established[11-15], the most recent works of which represent the state of the art. The present work extends the database by providing hundreds of dynamic interface events to initially quiescent low-g surfaces, each event requiring from 5s to 30s of low-g time to fully decay.

In this paper a description of the CL hardware is provided followed by the general experiment operating procedure. A list of the tests performed with pertinent statistics is provided prior to the description of the data reduction and organization methods. A representative subset of the flight data is then compared with blind numerical predictions employing the empirically determined perturbations. The short term impact of such comparisons is discussed in conclusion.

III. Description of CFE-CL Hardware

The two CL experiment units are envisioned with the principle design drivers of safety, a short delivery schedule, small mass (< 2kg each), small volume (< 2L each), no electrical power requirements, and minimal to no crew training requirements while providing a direct quantitative measure of the extremes in dynamic fluid interface behavior expected from an assumption of either a free or pinned contact line condition. A photograph of the CFE-CL-2 flight unit is provided in Figure 1 along with a solid model of the design with key dimensions noted. The two units are identical in all respects save wetting properties, fluid volume, and pinning lip location. The main body is machined from a single piece of cast acrylic and fitted with aluminum pistons and stainless steel piston drive screws. The right circular cylindrical test chambers have flat bases but elliptical acrylic lids.

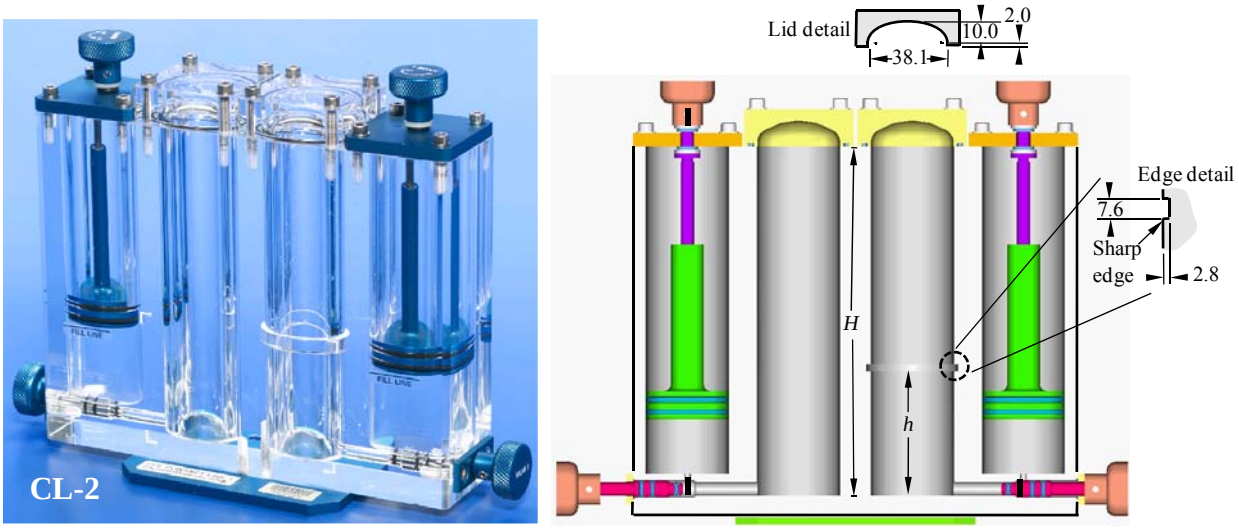

Figure 1. Image of CL vessel with critical dimensions (mm) identified on schematic at right.

Each unit is secured to an aluminum base plate with a single slotted hole that is used for attachment to the ISS MWA[16] via a captive fastener allowing for as much as 40mm lateral motion or adjustment. Turning a knob con-

nected to a drive screw displaces the piston. The knob diameter and screw pitch are selected so that a slow and stable manual fill process is assured. The double O-ring sealed reservoirs, charged at atmospheric pressure ($\approx P_{atm}$), hold the silicone oil test liquid and employ pistons to dispense the liquid into the respective test sections. Thus, the blind test chambers are somewhat pressurized ($\approx 1.3P_{atm}$) when the liquid is fully deployed. The design meets a single level of containment requirement for a 'zero-hazard' test liquid enabling the experiments to be performed by any crew member in the open ISS laboratories.

The general experimental objective is to fill the cylinders to identical levels with the same liquid establishing nearly identical interface configurations. The only difference between the interfaces in the different cylinders is that one of the contact lines is pinned at a pinning edge created by a groove machined into the cylinder walls (cylinder at right in Figure 1 with dimensions noted). Because the cylinders are closely and rigidly coupled, any disturbance imparted to the vessel produces nearly identical disturbances to both Smooth and Pinning cylinders. The disturbance input and response of the interfaces (i.e. frequency and damping rates) are quantified to at best ± 90μm and at worst ± 125μm from the video data (720x480px CCD at 30fps). Comparisons of the data for a variety of disturbances identify the physical bounds that can be expected for the assumptions of free and pinned contact line conditions. Idealizations of these limiting conditions are often imposed by numerical methods used to predict such phenomena and can lead to significant departures from observations[17,18,22]. As demonstrated herein, the quantified disturbances and resulting interface responses provide an adequate dataset to benchmark theoretical and/or numerical models.

The CL-1 unit tests a partially wetting liquid with contact angle of ~ 50º while the CL-2 unit tests a perfectly wetting (spreading), zero contact angle liquid. The selection of a 38.1mm cylinder diameter is constrained by an ISS safety requirement for maximum fluid volume. The cylinder diameter is sized to be as large as possible within this constraint to access uniquely low-g inertial-capillary regimes without introducing overbearing depth effects. The liquid volume and height of the pinning lip are selected such that the liquid depth from the centerline of the low-g menisci to the cylinder base is the same for both CL-1 and CL-2 at h = 31.75mm (depth/radius = 1.67). These and other container specifics are summarized in Table 1.

Table 1. Physical properties and important dimensions.

Physical Dimensions	
Pinning Lip Height (mm)	7.6 ± 0.1
Cylinder Height, H (mm)	146.0 ± 0.1
Cylinder Diameter (mm)	38.10 ± 0.05
Pinning Lip Diameter (mm)	43.7 ± 0.1
Refractive Index (Acrylic), N_D	1.491
θ = 50° (CL-1)	
Base to Pinning Lip, h (mm)	36.9 ± 0.1
Max Fluid Volume (mL)	39.04
θ = 0° (CL-2)	
Base to Pinning Lip, h (mm)	50.80 ± 0.1
Max Fluid Volume (mL)	43.44

Fluid Properties	ISS Temp. 25ºC
Fluid	Silicone Oil
Viscosity, ν	2 cst ± 2%
Density, ρ	872 ± 5 kg/m^3
Surface Tension, σ	0.0187 N/m ± 5%
Refractive Index, N_D	1.390
θ = 50° (CL-1)	
Advancing, θ_{adv}	52.2 ± 2°
Receding, θ_{rec}	47.3 ± 2°
Equilibrium, θ_{eq}	48.7 ± 2°

Certain wetting barriers are applied to the containers to enhance control during the experiment operations. The surface coating conditions vary between CL-1 and CL-2. The entire interior surface of CL-1 is rinse coated with FC-724, a transparent fluoro-polymer surface coating manufactured by 3M Corporation. CL-2 is intended to be a perfectly wetting experiment thus for the Pinning cylinder the interior surfaces above the pinning lip are coated, including the groove making up the pinning edge. The discontinuous wetting boundary established across the pinning lip in CL-2 creates a passive means of returning the fluid from above the pinning edge to below it via a favorable wetting discontinuity. The lid of the Smooth cylinder is also coated. All other surfaces of CL-2 are uncoated and exhibit perfect wetting, $\theta = 0°$. The equilibrium contact angle for the silicone oil on the FC-724 surface is determined by measuring advancing and receding contact angles using a tilted FC-724 coated glass capillary tube[19]. These values are listed in Table 1. The equilibrium angle is computed[20] to be 48.7 ± 2°, but is frequently referred to as 50º in reference to CL-1. Contact angle values identified during the flight experiments confirm these values despite the test unit being stored for approximately 2 years prior to testing.

IV. Procedures, Performance, and Sample Data

The CL experiments require up to 3 hours for set-up, complete nominal operations, and tear down. Continuous video coverage is not possible due to loss of contact with the ISS during its approximately 90 minute orbit. Nonethe-

less, during each performance, ample real-time video and audio downlink are available to provide the ground-based science team with a feeling similar to conducting the experiments in person. Following the experiments, the astronauts downlink continuous video data temporarily recorded on the onboard video system (VTR). All real-time and post-experiment downlink video data is stored on the ground for preliminary analysis despite its decreased resolution (due to compression) and reduced frame rate (as low as 8 frame/s). It is used to help specify subsequent tests and in some cases provides original data. The flight tapes (40 minute ISS DVCam videotapes) are returned to Earth and now serve as the source for all of the nominal resolution data reduction. Additionally, significant science events are recorded by downlink video during periods when the ISS camcorder is not operating. These data certainly compliment the flight tapes and are analyzed to all extents possible.

A typical experiment set-up is shown in Figure 2. The ISS camcorder is secured to the ISS rail, not the MWA, and aligned 'by eye' normal to the front face of the CL vessel. Any lack of orthogonality is corrected through image processing on the ground. A sheet of paper serves as a diffuse backlight screen. Sample static and dynamic images of the fluid interfaces taken from the flight video tapes are shown in Figure 3. As previously stated, because the two cylinders are rigidly and closely connected any disturbance imparted to the vessel is nearly identical to both fluid interfaces and significant differences in fluid response are largely a consequence of the different conditions at the contact line. As a case in point, simultaneous meniscus centerline location z and '½ radius' location ($\equiv R_{½}$) histories are digitized from the video data and presented in Figure 4 for both Smooth and Pinning cylinders in response to axial and slosh (Push) disturbances, respectively (refer to Figure 3 for notation). The disturbances to the containers shown in the insets and the general data reduction methods will be discussed shortly. It is clear by even casual inspection of Figure 4 that the fluid response is strongly dependent on the contact line boundary condition. (Note: For large amplitude Axial disturbances, the centerline location of the interface is often obscured from view and thus experimental data can only be collected in such cases after the disturbance has ceased, i.e. Figure 4, left.)

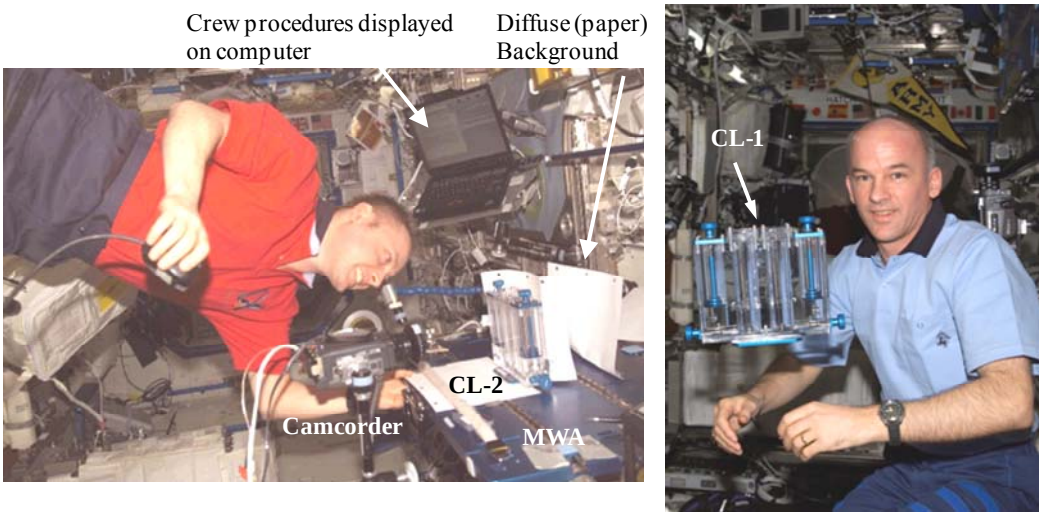

Figure 2. Astronauts M. Fincke (left) and J. Williams (right) on ISS during CFE-CL experiments.

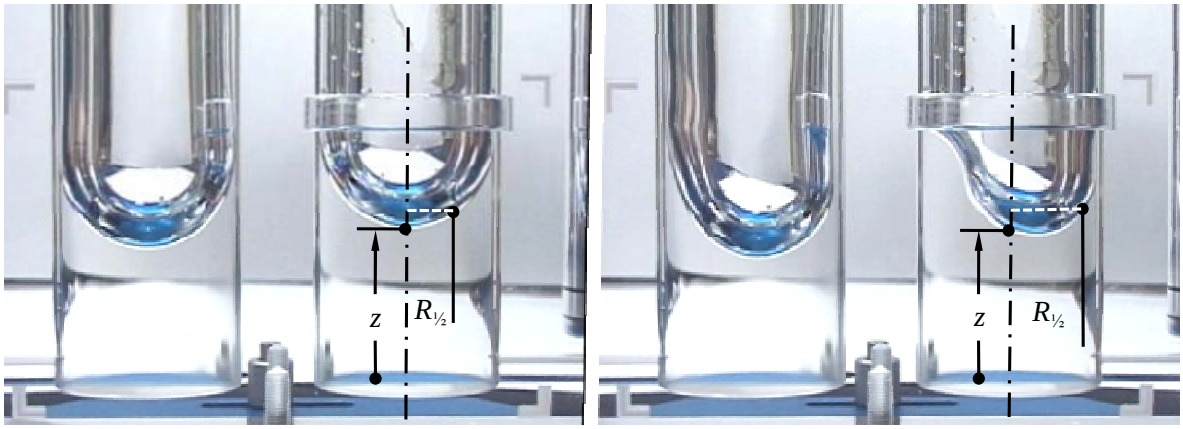

Figure 3. Typical quiescent initial conditions (left) and dynamic nonlinear response (right) for CL-2.

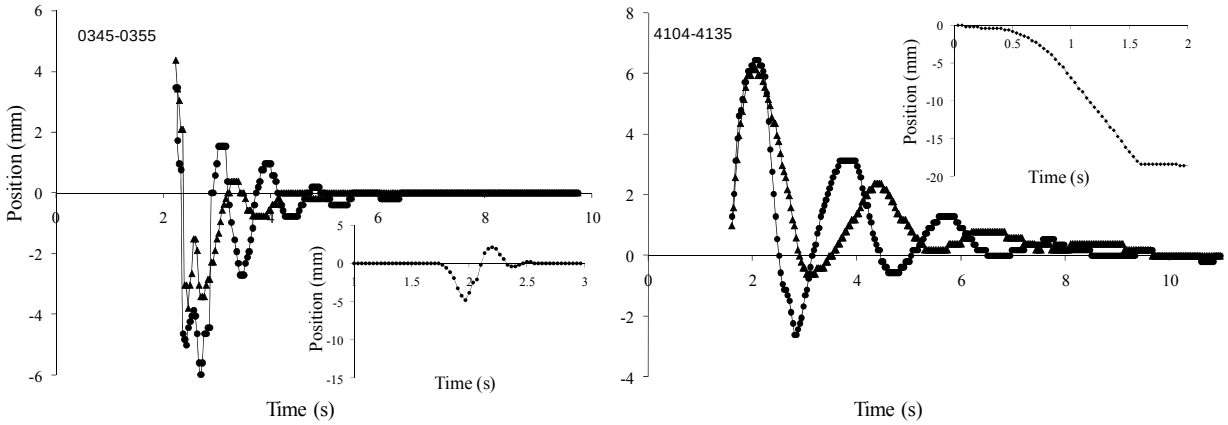

Figure 4. Superposition of simultaneous Smooth (triangles) and Pinning (circles) cylinder interfaces to Axial $z(t)$ (left) and Push $R_{½}(t)$ (right) disturbances. Disturbance data shown in inset.

The general experimental procedures are as follows: After observations of the liquid interface in response to the natural ISS background g-environment (typically ~ $10^{-5}g_o$) the astronaut manually imparts several disturbance types to quiescent low-g surfaces. (Note: the background g-level of the ISS did not produce detectable disturbances to the interface.) The disturbance types pertinent to CL include Tap, Push, Slide, Multislide, and Swirl, and are briefly described here:

- Tap: Solitary Taps (impulses) of gradually increased magnitude are imparted to the rigidly mounted test vessel beginning with the pad of a finger and ending with light raps with a knuckle. Low amplitude high frequency damped oscillations of the interfaces are observed that can only be marginally resolved from the flight tapes.
- Axial: Axial mode disturbances are imparted to a CL vessel fixed to the MWA by displacing and releasing the MWA table itself, much like a diver does to a diving board (refer to inset, Figure 4, left). The MWA thus serves as a highly damped cantilever imparting axial disturbances of easily variable amplitude to the cylinders. Linear and nonlinear axial perturbations are imparted in this manner with amplitudes increasing to the point of drop ejection (ejected drop diameters ~ 15mm).
- Push: The screw fastening the CL unit to the MWA is loosened for this disturbance such that the vessel may slide left to right in the field of view yet remain flush with the MWA surface. The Push disturbance is an impulse-like disturbance leading to damped slosh-mode oscillations of the interface (ref. Figure 4, right). The Push is imparted by finger across the field of view, gradually increasing the disturbance amplitude from linear to nonlinear regimes.
- Slide: Similar to the Push, the Slide disturbance is a single full-period lateral oscillation completed within the field of view at the approximate natural frequency of the interfaces. The peak-to-peak amplitude of the full period disturbances is varied while the frequency of the Slide is held approximately constant.
- Multislide: A Multislide disturbance is defined as a multiple (2, 3, 4+) period lateral oscillations completed within the field of view at the approximate natural frequency of the interfaces. The peak-to-peak amplitude of the full period disturbances is varied while the frequency of the Multislide is held approximately constant.
- Swirl: The Swirl disturbance is defined as a swirling slosh mode induced to the fluid using an elliptical or circular sliding motion of the CL vessel in the plane of the MWA. The fastener is removed for these tests. The Swirl disturbance diameter is approximately 30 to 40mm with swirl periods increasing incrementally from 1 to 5. The larger amplitude Swirl disturbances yield centrifugal force-dominated vortical flows.

Care is taken to postpone disturbances that de-pin the Pinning cylinder interface. A 'wait time' is specified between each disturbance for all visible interface oscillations to decay, typically 5-60 seconds. In general, destabilized interfaces can be reconfigured at will using a manual astronaut-defined centrifugal method, but at the cost of up to 10 minutes of crew time.

Because the disturbances are imparted manually, the possibility of precisely repeating a given disturbance is unlikely. Nonetheless, 3-D image analyses are used to quantify the frequency and amplitude of each disturbance such that all disturbance inputs are known with sufficient accuracy. The Tap, Axial, Push, Slide and Multislide dis-

turbances result in damped axial or slosh-type oscillations that are readily compared for both Smooth and Pinning cylinders. For brevity, only sample results for the Axial and Push disturbances are presented herein.

V. Brief Summary of Science and Extra-Science Results

Hundreds of individual data sets for CFE-CL were recorded towards the primary science objectives. Many additional 'tests' were also conducted for what is considered 'extra science.' A chronology of experimental efforts by the astronauts is outlined below:

- 1st Performance CL-2 (Fincke): Nominal Science Run
  - Successful completion of all science objectives
  - Demonstration of centrifugal technique to reset experiment for certain repeat runs
  - Identified controlled method to impart axial mode disturbance using MWA
  - Noteworthy additional science: droplet ejection, drop-wall impacts and rebound, hourglass formation in Smooth cylinder
- 2nd Performance CL-2 (Fincke): Extra Science
  - Repeat Push, Slide, and new data using Axial mode
  - Noteworthy additional science: Depth effects to Push disturbance
- 3rd Performance CL-2 (McArthur): Extra Science
  - Demonstrate augmented version of Fincke centrifuge method to fully clear pinning lip of liquid allowing for the indefinite repetition of the experiments
  - Repeat Push, Slide, and Axial mode (camera mounted to MWA)
  - Noteworthy additional science: more droplet/jet ejections, drop-wall impacts, and rebound
- 4th Performance CL-2 (J. Williams): Extra Science
  - Perfection of McArthur's augmented centrifuge method
  - Repeat Push, Slide, and Axial mode (camera mounted ISS rail)
  - Noteworthy additional science: significant droplet/jet ejections and manifold droplet-wall and free surface impacts and rebound events
- 1st Performance CL-1 (J. Williams): Nominal Science Run
  - Successful completion of all science objectives
  - Noteworthy additional science: some depth effects
- 2nd performance CL-1, (Whitson): Extra Science
  - Large amplitude axial mode pinned oscillations and destabilizations
  - Larger accelerations than could be imparted by hand were required to clear pinning edge of liquid. Experiment terminated prematurely

In addition to the now considered foundational Axial-mode tests, which were conceived on orbit and originally considered as 'extra science,' a significant number of extra science measurements and observations are made of dynamic interfacial phenomena of both general and practical interest. Some of these tests are highly complementary to the CFE-CL investigation, such as liquid depth effects to axial and slosh-type disturbances. Others tests, such as the behavior of ejected drops and their impacts with solid and fluid surfaces, have nothing to do with the original CL science objectives. Several such 'extra science' tests are reported elsewhere all of which yield quantitative data[3]. A detailed summary of 'extra-science' CFE-CL data is anticipated in a subsequent publication.

VI. Status of Data Reduction, Analysis, and Organization

The CL data reduction and organization effort has been underway for over three years. The video sources consist of real-time downlink video and VTR dump video in addition to the actual ISS camcorder flight video tapes recently returned to Earth. Approximately 90% of such data employs the highest resolution onboard video tape data. Approximately 95% of the CL primary science data has been extracted and is now in the process of being analyzed to provide large sample statistics. At present, over 350 individual tests have been digitized including approximately 30 extra science events. These include approximately 72 Axial, 36 Push, 3 Slide, and 14 Multislide disturbances for CL-1 and approximately 44 Axial, 50 Push, 53 Slide, and 92 Multislide disturbances for CL-2. A database is under construction that links each dataset (i.e. test number, test container, disturbance type, etc.) to the digitized data tables and plots of both the input disturbance and fluid response, as well as to the original image (i.e. video file) of the event. The CFE-CL video library alone might be all that is necessary for one to benchmark a particular model. All details associated with the data reduction such as image analysis protocol, coordinate origins, scale factors, etc. are provided in the database, which is under development with the intention of being made publicly available via university server. A thorough analysis should be successfully conducted with these information sources.

VII. Sample Blind Numerical Predictions, Comparisons, and Discussion

Because the CL dataset provides a unique opportunity to benchmark such analytical predictions, as a demonstration of this process and the use of the CL data to this end, blind numerical computations are conducted of select CL datasets using the empirically applied input disturbances. This exercise serves as an authentic test of current capabilities to predict sensitive phenomena rarely verified by experimental data. The degree of success of such computations is not without practical implications. A brief overview of the numerical approach selected is provided here prior to comparisons of specific cases.

Several numerical methods have been applied to the general problem of large length scale capillary reorientation in right circular cylinders, including at least FIDAP[21,22], Flow3D[3,23], and now OpenFoam[24]. The latter is employed in this analysis with the OpenFoam CFD toolbox, an object-oriented C++ open source library supplied with a complete set of pre-configured solvers and utilities. The implemented, incompressible two-phase Navier-Stokes solver *interFoam*, which tracks the interface using a VOF method, is chosen for the model. All computations in this work are conducted on three commercial computers, i.e. single core 2.8GHz, 32-bit, Intel Pentium 4 processors, with 1GB RAM. The majority of the somewhat optimized computations typically run overnight or longer requiring approximately 2 hours of computation time for each second of actual 'experiment' or 'flow' time (herein denoted for example as ~ 2hr/s).

In keeping with the blind analysis concept, only fluid properties, test cell dimensions, and precise disturbance information are provided to the numerical analyst. Sample empirically determined disturbance data is presented in Figure 5 in the form of CL container position as a function of time. The data is first smoothed (Figure 5, left) and then differentiated twice to obtain the time dependent acceleration (Figure 5, right). A time-varying body force vector is then implemented in the interFoam solver to model the input disturbance. It will be shown that the smoothing algorithm applied to the input disturbance has negligible impact on the fluid response (cf. Figure 7, left).

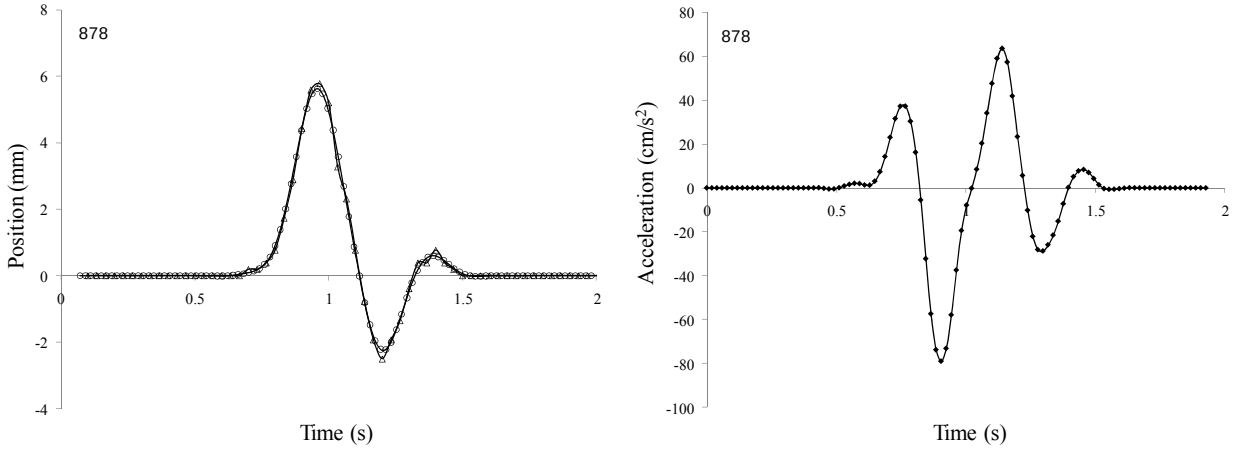

Figure 5. At left, sample raw (open triangles) and Loess smoothed (open circles) position data (open triangles). Resulting acceleration profile using smoothed data shown at right. Axial disturbance is for CL-2, assumed identical for both Smooth and Pinning cylinders.

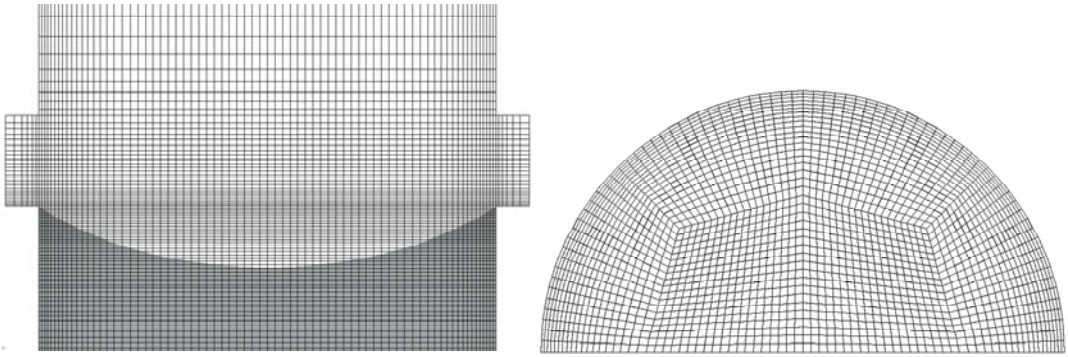

Figure 6. Computational grid for the Push simulation (CL-1, θ = 50º, Pinning cylinder): extruded layers with refinements at the pinning edge and initial fluid interface at left, cross-sectional half domain using quadrangles at right (Blockmesh).

Because the computations are blind, grid resolution, refinement, and optimization must be decided without the aid of the experimental results themselves. Thus, low-resolution pre-calculations are performed to assess the general fluid response to the experimentally provided disturbance in order to select the appropriate mesh and mesh refinements in regions of highest velocity gradients and in particular near the contact line. This exercise also provides an estimate of the experiment 'flow' time. The pre-calculations employ 10,000 cells and require approximately 30 minutes each. Subsequent to such calculations, a grid-type is chosen for the most optimal computations. In this case the computational mesh has been modeled by 100,000 hexaeders, using the implemented *blockMesh* grid generator. As shown in Figure 6, there are local refinements near the free surface and the contact line. Without the advantage of fluid specific contact line data available a priori a constant contact angle is specified as the moving contact line boundary condition. Though there are certainly physical grounds in support of this boundary condition at nano-scales[7], its application at the 'milli-scale' of the numerical domain might raise some suspicion. Nonetheless, this boundary condition has proven successful in previous studies[14,15] and naturally accommodates the pinned contact line condition at an abrupt edge.

Further computational details are presented in Figure 7 for CL-2 in response to an Axial disturbance. Figure 7 (left) demonstrates that the numerical results for the interface response are essentially independent of the Loess smoothing interpolation function of the empirically derived input disturbance. The highest smoothing function was employed for all calculations. To determine the dependence of the solutions to the chosen computational grid, an additional cross-sectional pattern was examined. The second mesh is generated automatically with the open source grid generator *Gmsh*[25] using a mixed grid with prisms and hexaeders and again local refinements at the contact line. The comparison is presented in Figure 7 (center). It is clear from observations of the figure that the results converge as the resolution increases. However, the computational time required for the structured grid in Figure 6 (Block-Mesh-Fine) is 50% that of the automatically generated grid for equivalent accuracy. The structured grid is selected for all computations on these grounds. Lastly, In Figure 7 (right) a grid resolution study demonstrates the general convergence of the solution with increased mesh refinement and that the 100,000 cell model at 2.14 hr/s (L = 0.63mm) computational time is a practical choice over the 200,000 model at 8.08hr/s (L = 0.5mm), especially considering that certain events require greater than 15s of flow time. The experimental CL-2 data for this test case is provided post-computations for reference. It should be noted that the increased refinement leads to increased agreement with the data and that even low grid densities produce potentially adequate results for design purposes (i.e. 10,000 cells with L = 1.37mm yields 0.15hr/s computational time, while 30,000 cells with L = 0.94mm yields 0.57hr/s). The ½-domain is solved for the slosh mode disturbances while the ¼-domain is solved for axial modes. It is also important to note that all numerical computations are carried out for CL-1 with $\theta = 50^{\circ}$, despite the experimentally determined value of $\theta = 48.7 \pm 2^{\circ}$ with notable hysteresis, Table 1.

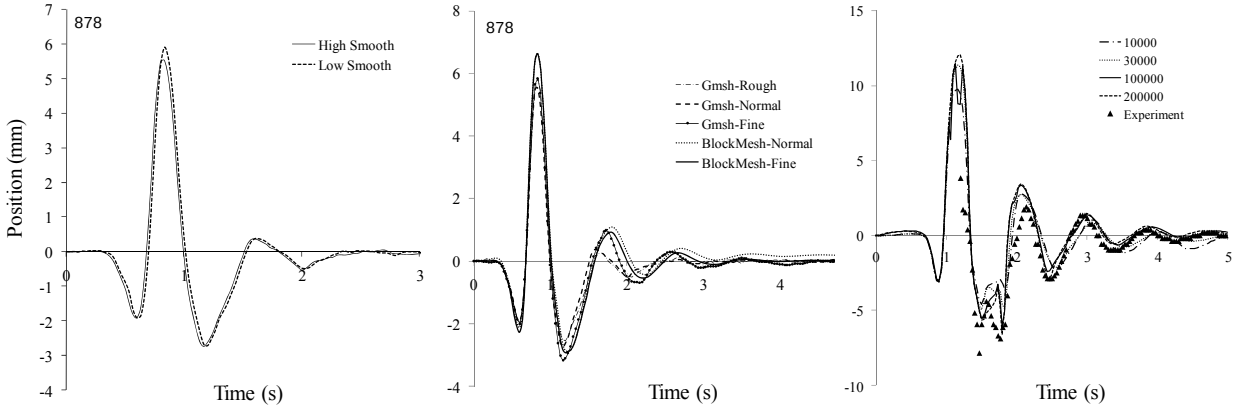

Figure 7. Assessment of numerical approach for typical Axial disturbance to CL-2: (left) the impact of the smoothing algorithm to the input disturbance (ref. Fig. 5) is negligible, (center) solutions for two mesh generators at various refinements reveal BlockMesh-Fine is most accurate per unit computational time, and (right) convergence of the solution with increasing number of grids.

VIII. Comparisons and Discussion

Sample computations are presented in Figures 8-11 for CL-1 ($\theta = 50^{\circ}$) and CL-2 ($\theta = 0^{\circ}$), for Axial and Push disturbances, and for both Smooth and Pinning cylinders. The circles are the numerical predictions and the triangles are the experimental data. The disturbance profiles are presented on each plot (see insets). The Axial disturbance comparisons overlay the meniscus centerline history $z(t)$ with that determined for the experiments. The Push distur-

bance comparisons overlay the lateral location of the 'optical' ½ radius location of the interface profile $R_{½}(t)$ as identified in Figure 3 (right). Due to an index of refraction mismatch between the liquid and the acrylic container a ray trace correction is employed to shift the location of the numerically determined ½ radius location such that both numerical and experimental '½ radius' locations are coincident. (Experiment measurements for Push disturbances are made at $r = 0.952$cm ($= 0.5R$, where $R = 19.05$mm), but must be corrected for optical distortion such that the true radial location of such measurements is $r = 9.87$mm. The numerical '½ radius' location uses the latter location for the comparisons.).

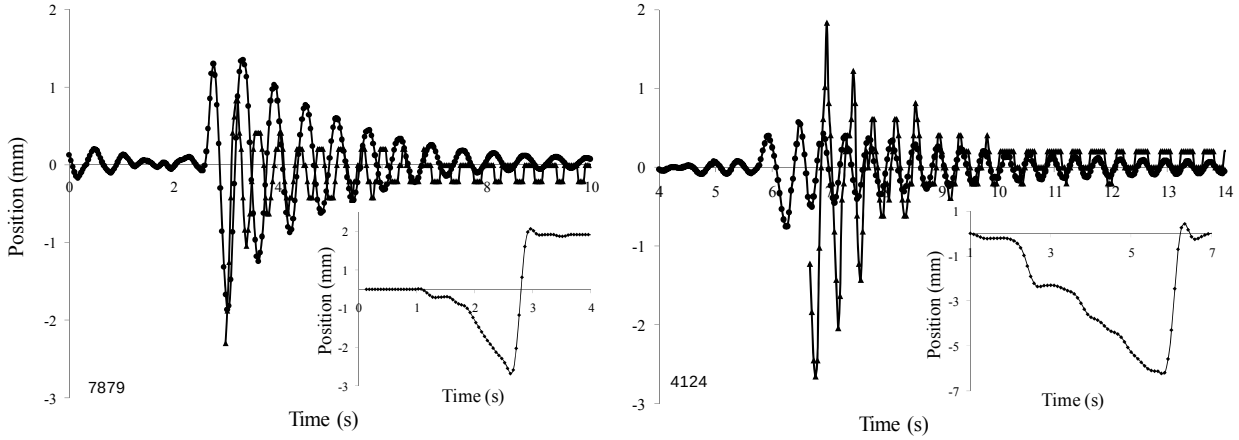

Fig. 8. CL-1 ($\theta = 50°$) Axial: Smooth (left), Pinned (right).

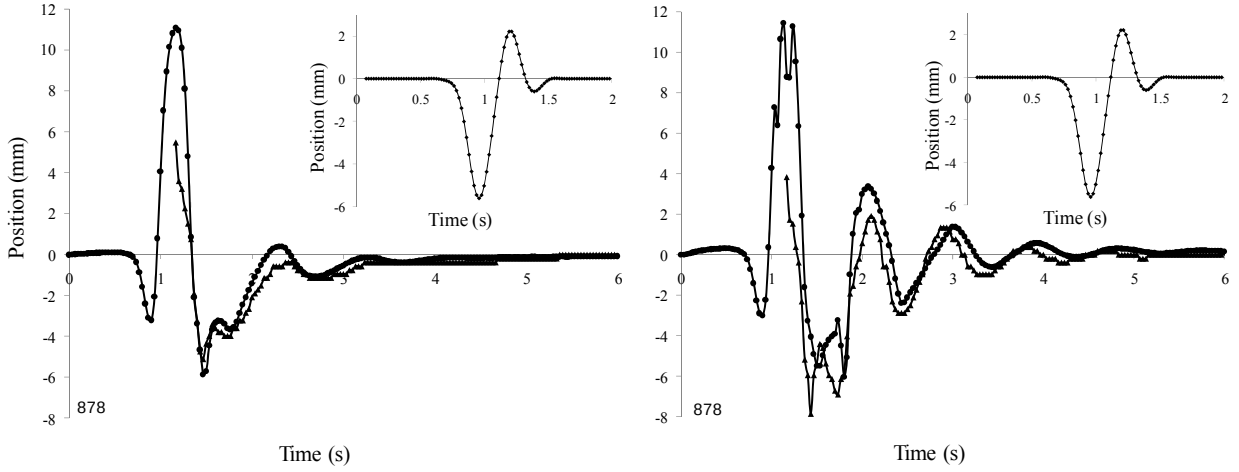

Fig. 9. CL-2 ($\theta = 0°$) Axial: Smooth (left), Pinned (right), note identical disturbance (inset).

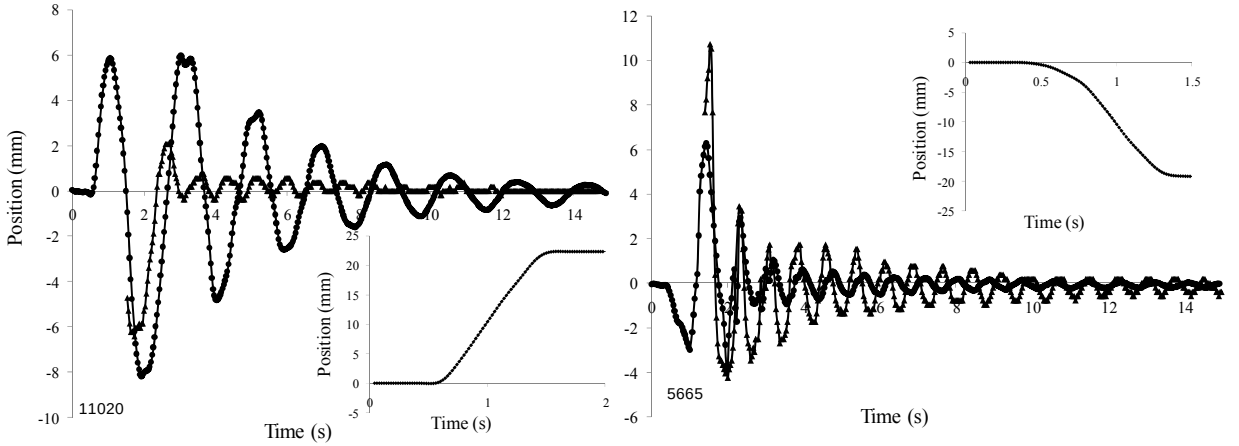

Fig. 10. CL-1 ($\theta = 50°$) Push: Smooth (left), Pinned (right).

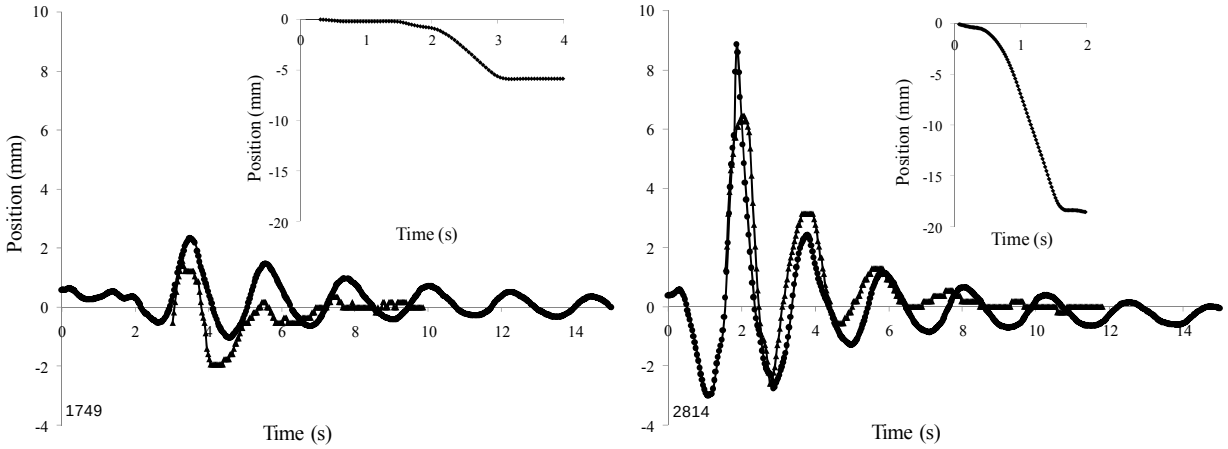

Figure 11. CL-2 (θ = 0º) Push: Smooth (left), Pinned (right).

Table 2. Comparisons of select experimental and numerical results from Figures 8-11.

	f_{exp}	f_{num}	ζ_{exp}	ζ_{num}	N_{exp}	N_{num}	A_{exp}	λ_{nl}	λ_l
	Hz (± 1%)	Hz (± 1%)	s^{-1} (± % err.)	s^{-1} (± % err.)			(mm)		
θ=50° (CL-1)									
Axial: Pinned	2.48	2.47	1.06 (6)	0.30 (2)	25	33	4.5	5.31	1.81
Smooth	2.50	1.66	0.33 (5)	0.51 (1)	24	20	3.1	-	0.61
Push: Pinned	1.31	1.17	0.20 (3)	0.19 (5)	21	11	15.0	1.75	3.13
Smooth	1.24	0.54	0.27 (7)	0.25 (1)	11	8	8.5	0.35	0.16
θ=0° (CL-2)									
Axial: Pinned	1.13	1.11	1.11 (4)	1.04 (3)	3	5	9.8	1.36	0.57
Smooth	1.25	0.91	1.00 (-)	1.20 (-)	2	2	5.5	0.79	-
Push: Pinned	0.56	0.45	0.62 (4)	0.17 (3)	4	5	9.1	0.80	0.60
Smooth	0.43	0.48	0.54 (-)	0.72 (-)	3	3	3.5	1.50	3.85

Several key characteristics of the dynamic interface response are compiled in Table 2. Included are experimental and numerical values for linear natural frequency f, linear damping rate ζ, number of periodic nodes N used in determining the damping rate and frequency, and maximum nonlinear and linear experimental vs. numerical amplitude ratios λ. The amplitude ratios provide a measure of the accuracy of the maximum computed amplitude of the interface oscillations compared to those observed in the experiment. The linear regime is defined by oscillation amplitudes less than ~ 0.1R (approximately 2mm). The damping rate ζ is defined here as the best fit to the decay function $\exp^{-\zeta t}$ in the linear regime. A_{exp} provides an assessment of the nonlinearity of the perturbation as the absolute peak-to-peak amplitude of the first experimentally determined oscillation in millimeters. Note that all values for A_{exp} in Table 2 are greater than 2mm below which deflections are considered fully linear.

As can by observed from the comparisons by inspection, in general, the numerical results are in surprisingly favorable agreement. Experimental frequencies between 0.43 and 2.50Hz, damping rates between 0.20 and 1.11s^{-1}, and maximum interface deflection ratios between 0.35 and 5.31 are listed. Not listed in the table are dynamic Bond numbers ($Bo = \rho a R^2/\sigma$, where a is the local acceleration, ρ if the liquid density, and σ is the surface tension) which vary between 0.42 and 13.2 for the tests presented. Several important observations from the comparisons are provided below:

- As expected, for a given cylinder the Axial disturbance natural frequency is approximately twice that of the first sub-harmonic Push disturbance (slosh) frequency.
- As expected, for a given disturbance the CL-1 (θ = 50º) natural frequency is approximately twice that of CL-2 (θ = 0º).
- In part as expected, for the Push disturbance the Pinning cylinder natural frequency is approximately twice that of the Smooth cylinder.

- In general, agreement is most favorable for the perfectly wetting condition (CL-2), Figures 9 and 11. This is in part due to the highly damped nature of the resulting flows, which naturally reduces the sensitivity of the flow to the boundary condition applied at the contact line—Smooth and Pinning cylinders respond similarly. The Axial disturbance is well predicted as might be expected from previous numerical experience[14,15] but the Push disturbance is replicated only 'reasonably well' with discrepancies of ~ 20% in natural frequency and under-predictions of damping rates by a factor of 3.6 (see Smooth cylinder case in Figure 11, right).
- The most quantitative agreement in terms of oscillation amplitude, frequency, and decay rate is achieved for the Axial disturbance and the perfectly wetting condition (CL-2) for both Smooth and Pinning cylinders, Figure 9.
- Discrepancies arise most noticeably for the partial wetting case (θ = 50º, CL-1), where despite the poorer agreement the Pinning cylinder results fair better than those of the Smooth cylinder. The increased inaccuracy is primarily due to the choice of contact line boundary condition, and is readily observed over the manifold weakly damped oscillations, Figure 8. The Axial disturbance is more amenable to the present choice of boundary conditions, but still leads to 33% under-predictions in amplitude for the Smooth case and 3-fold over-predictions of damping rate for the Pinned case.
- The least quantitative comparisons arise for the partial wetting case (θ = 50º, CL-1) and Push disturbance where ~ 2 to 3-fold over-predictions in interface amplitude and ~ 50% under-predictions of frequency are observed, Figure 10. The pinned condition of the contact line is more appropriate as the boundary condition for the Smooth cylinder in this case and would largely correct the frequency error. Such wetting conditions demand a model incorporating advancing and receding contact angle data. One such model was attempted[14], but found to be initially incompatible with OpenFoam. It is perhaps coincidental, but despite the disagreement in amplitude and frequency, the damping rate is in good agreement for such cases with errors ~ 5%.

Several practical conclusions may be drawn for these low-mode oscillation comparisons: (1) The current OpenFoam model does surprisingly well to predict the large length scale capillary phenomena for highly wetting systems with a simple fixed contact angle boundary condition at the contact line. (2) The model may be successfully tuned via pre-calculations improving the likelihood of accurate and efficient 'blind' computations for design and analysis. (3) The greatest efforts to further improve the general numerical approach should focus on the boundary conditions necessary to specify partial wetting systems with contact angle hysteresis. Spacecraft fluid systems employing such fluids (i.e. water processing systems) will likely require parametric studies for the various conditions that can arise at the contact line represented in their extreme cases by perfect slip and perfectly pinned conditions.

IX. Current Summary and CFE-CL Directions

The handheld CFE-CL experiments recently completed aboard ISS serve as a benchmark for numerical models used to design and analyze large length scale capillary systems common on spacecraft. The CL experiments demonstrate pinned and free contact line boundary conditions for a variety of disturbances to quiescent low-g interfaces including axial, slosh, and swirl modes. Axial and slosh (i.e. Push) disturbances are reported herein. A sample of digitized flight test results is presented as indicative of what is to be made publicly available on permanent archive including a video library with digitized disturbance and interface response data. A selection of the flight tests are predicted in-the-blind using CFD. The encouraging preliminary agreement improves confidence in current numerical methods to predict capillary dynamics in highly wetting scenarios (i.e. tankage for fuels and cryogens). The comparisons also imply that more work is required to establish similar confidence in partial wetting scenarios that depend more substantially on the moving contact line boundary condition (i.e. water processing systems).

Acknowledgment

The authors are deeply indebted to astronauts Michael Fincke, William (Bill) McArthur, Jeff Williams, and Peggy Whitson for successful space experiments performed on ISS, Expeditions 9, 12, 13, and 16, respectively. In several instances the experiments were performed during the crew's personal time as Voluntary Science. The authors would also like to thank the NASA support cadre at JSC, MSFC, and especially GRC for assistance during the mission and in meeting the demanding development schedule. Special thanks are due to Charles Bunnell of Zin Technologies for an enduring commitment to the engineering success of CFE. This work is supported in part by NASA through contract NNC05AA29A and by the Federal Ministry of Economy and Technology (BMWi) through the German Aerospace Center (DLR) under grant number 50 WM 0535.

References

[1]Weislogel, M.M., Collicott, S.H., Gotti, D.J., Bunnell, C.T., Kurta, C.E., Golliher, E., The Capillary Flow Experiments: Handheld Fluids Experiments for the International Space Station, AIAA-2004-1148, 42nd AIAA Aerospace Sci. Mtg. and Exhibit, Reno, Nevada 5-8, Jan. 2004.

[2]Weislogel, M.M., Bunnell, C.T., Kurta, C.E., Golliher, E.L., Green, R.D., Hickman, J.M., Preliminary Results from the Capillary Flow Experiment on ISS: the Moving Contact Line Boundary Condition, Paper No. AIAA-2005-1439, 43rd AIAA Aerospace Sci. Meeting and Exhibit, Reno, Nevada 10-13, Jan. 2005.

[3]Weislogel, M., Jenson, R., Klatte, J., Dreyer, M., Interim Results from the Capillary Flow Experiment Aboard ISS: The Moving Contact Line Boundary Condition. AIAA-2007-747, 45th AIAA Aerospace Sci. Meeting and Exhibit, Reno, Nevada, Jan. 8-11, 2007.

[4]Dussan V, E.B., On the Spreading of Liquids on Solid Surface Static and Dynamic Contact Lines, *Ann. Rev. Fluid Mech*., 1979 11:371-400.

[5]Davis, S.H., Contact Line Problems in Fluid Mechanics, *J. of Appl. Mechanics*, Vol. 50/977-982, Dec. 1983

[6]Kistler, S.F., Hydrodynamics of Wetting, in Wettability, *Surfactant Science Series*, Vol. 49, edited by J.C. Berg, 1993, pp 311-430.

[7]Koplik, J., Banavar, J.R., Continuum Deductions from Molecular Hydrodynamics, *Ann. Rev. Fluid Mech*., Vol. 27, 1995, pp. 257-292

[8]Ramé, E., Moving Contact Line Problem: State of the Contact Angle Boundary Condition, Encyclopedia of Surface and Colloid Science, pp 3602-3618, Marcel Dekker, Inc. 2002.

[9]Shikhmurzaev, Y.D., Capillary Flows with Forming Interfaces, Chapman and Hall/CRC, 2008.

[10]Weislogel, M.M., Survey of Present and Future Challenges in Low-g Fluids Transport Processes, NASA Contract Report C-74461-N, TDA Research, Wheat Ridge, CO, 2001.

[11]Siegert, C.E., Petrash, D.A., Otto, E.W., Time Response of Liquid-Vapor Interface after Entering Weightlessness, NASA TN D-2458, 1964.

[12]Weislogel, M.M., Ross, H.D., Surface settling in partially filled containers upon step reduction in gravity, NASA Technical Memorandum 103641, Lewis Research Center, Cleveland, OH, November, 1990.

[13]Weislogel, M., Fluid Interface Phenomena in a Low-Gravity Environment: Recent Results from Drop Tower Experimentation, *Space Forum*, Vol. 3, pp. 59-86, Gordon & Breach, Amsterdam, Netherlands, 1998.

[14]M. Michaelis, M.E. Dreyer, H.J. Rath, Experimental Investigation of the Liquid Interface Reorientation upon Step Reduction in Gravity, *Annals of the New York Academy of Sciences* 974:246-260 (2002).

[15]Dreyer, M. E., Free Surface Flows under Compensated Gravity Conditions, Series: Springer Tracts in Modern Physics, Vol. 221: Springer-Verlag (2006).

[16]The Maintenance Work Area (MWA) provides a rigid surface on which to perform maintenance tasks on ISS. The MWA consists of a blue anodized aluminum folding tabletop and two detachable arms. The arms attach to the seat track, providing the table with two solid connection points.

[17]Hocking, L.M., Waves produced by a vertically oscillating plate, *J. Fluid Mech*., Vol. 179, pp. 267-281, 1987.

[18]Ting, C.L., Perlin, M., Boundary Conditions in the vicinity of the contact line at a vertically oscillating upright plate: an experimental investigation, *J. Fluid Mech*., Vol. 2, pp 263-300, July 1995.

[19]Weislogel, M.M., Spontaneous Steady Capillary Flow in Partially Coated Tubes, **AIChE J**., 43, No. 3, March 1997, pp. 645-654.

[20]Tadmor, R., Line Energy and the Relation between Advancing, Receding, and Young Contact Angles, *Langmuir*. Vol. 20, No. 18, pp. 7659-7664, 2004.

[21]ANSYS, Inc., FIDAP Flow Modeling Software, http://www.fluent.com

[22]Wölk, G., Dreyer, M., Weislogel, M.M., Rath H.J., Damped Oscillations of a Liquid/Gas Surface Upon Step Reduction in Gravity, *J. of Spacecraft and Rockets*, 34, No. 1, pp. 110-117, Jan.-Feb. 1997.

[23]Flow Science Inc., FLOW-3D Modeling Tool, http://www.flow3d.com

[24]OpenFoam, the open source computation fluid dynamics toolbox, 2007, version 1.4, OpenCFD Ltd, Berkshire, UK: http://www.opencfd.co.uk/openfoam/index.html

[25]Geuzaine, C., Remacle, J.F., Gmsh—a 3-dimensional finite element mesh generator, Version 2.0.8, 2007: http://www.guez.org/gmsh